SCIENCE CHINA
Chemistry

•ARTICLES•

July 2018 Vol.61 No.7: 830–835
https://doi.org/10.1007/s11426-018-9234-2

A stable metal-covalent-supramolecular organic framework hybrid: enrichment of catalysts for visible light-induced hydrogen production

Xiong-Fei Li[1], Shang-Bo Yu[1], Bo Yang[1], Jia Tian[1], Hui Wang[1], Dan-Wei Zhang[1], Yi Liu[2*] & Zhan-Ting Li[1*]

[1]*Department of Chemistry, Collaborative Innovation Centre of Chemistry for Energy Materials (iChEM), Shanghai Key Laboratory of Molecular Catalysis and Innovative Materials, Fudan University, Shanghai 200438, China;*
[2]*The Molecular Foundry, Lawrence Berkeley National Laboratory, Berkeley, California 94720, USA*

Received January 26, 2018; accepted February 28, 2018; published online April 11, 2018

Cubic metal-covalent-supramolecular organic framework (**MCSOF-1**) hybrid has been created from the reaction of two molecular components and subsequent co-assembly with cucurbit[8]uril (CB[8]) in water. In the presence of CB[8], $[Ru(bpy)_3]^{2+}$-based acylhydrazine **1**·2Cl reacted with aldehyde **2**·Cl to quantitatively yield six-armed precursor **3**·8Cl through the generation of **MCSOF-1**. **MCSOF-1** combines the structural features of metal-, covalent- and supramolecular organic frameworks. Its periodicity in water and in the solid state was confirmed by synchrotron X-ray scattering and diffraction experiments. **MCSOF-1** could enrich discrete anionic polyoxometalates (POMs), maintain periodicity in acidic medium, and remarkably facilitate visible light-induced electron transfer from its $[Ru(bpy)_3]^{2+}$ units to enriched POMs, leading to enhanced catalysis of the POMs for the reduction of proton to H_2 in both aqueous (homogeneous) and organic (heterogeneous) media.

supramolecular organic framework, self-assembly, cucurbitu[8]ril, photocatalysis, hydrogen production

Citation: Li XF, Yu SB, Yang B, Tian J, Wang H, Zhang DW, Liu Y, Li ZT. A stable metal-covalent-supramolecular organic framework hybrid: enrichment of catalysts for visible light-induced hydrogen production. *Sci China Chem*, 2018, 61: 830–835, https://doi.org/10.1007/s11426-018-9234-2

1 Introduction

In the past decades, crystalline metal organic frameworks (MOFs) and covalent organic frameworks (COFs) have received much attention due to their great potentials for the development of various advanced materials [1−12]. We and others have recently created the self-assembly strategy for the generation of water-soluble supramolecular organic frameworks (SOFs) at room temperature from preorganized molecular components and cucurbit[8]uril (CB[8]) [13−20], with hydrophobicity as the driving force [21−28]. As a family of ordered porous supramolecular polymers [29−38], 3D SOFs have been demonstrated to exhibit robust capacity for time-dependent guest-adsorption in water [14,15,39,40]. Further development of new self-assembly methodology would facilitate the fabrication of new architectures that might display interesting functions. Here we describe that the formation of the inherently reversible hydrazone bonds can be utilized to direct three molecular components to react and co-assemble to produce a water-soluble 3D periodic metal-covalent-supramolecular organic framework (**MCSOF-1**) hybrid, which bears the structural features of the three kinds of frameworks. We further demonstrate that **MCSOF-1** could exist in solution and the solid state and enrich various anionic polyoxometalates (POMs) at very dilute concentration, which remarkably enhanced visible light-initiated

*Corresponding authors (email: yliu@lbl.gov; ztli@fudan.edu.cn)

multi-electron injection from its $[Ru(bpy)_3]^{2+}$ subunits to the adsorbed POM anions, leading to efficient reduction of proton to produce hydrogen in both aqueous (homogeneous) and organic (heterogeneous) media.

2 Results and discussion

Compound **3**·8Cl, which was formed from the reaction of **1**·2Cl and **2**·Cl, was designed as a hexatopic building block to interact with CB[8] to form **MCSOF-1** (Scheme 1). To evaluate the stability of **3** in water, the ^{1}H NMR spectra of **1**, **2** and their 1:6 mixture in D_2O were recorded (Figure S1, Supporting Information online). Both **1** and **2** exhibited two sets of signals. For **1**, this was attributed to the configurational isomerization of the hydrazide units, as indicated by variable-temperature ^{1}H NMR experiments (Figure S2). For **2**, this was ascribed to partial hydration of the aldehyde group into acetal (~15%) in D_2O, because this was not observed in DMSO-d_6 in both ^{1}H and ^{13}C NMR (Figures S3, S4). ^{1}H NMR of the mixture revealed that the reaction of **1** and **2** reached equilibrium after about 72 h (Figure S5). Based on the integration of the above two signals and that of the α-H (around 9.35 ppm) of the pyridinium unit of **2**, it was determined that ~53% of the hydrazine groups was converted to hydrazones. Assuming that the acylhydrazine units of all possible components possessed the identical reactivity, this conversion amounts to only a small fraction (4.2%) of **3** in the mixture of hydrazone products. When **2** of the same concentration was subjected to the reaction with 1.0 equiv of **4**, ^{1}H NMR showed that their reaction occurred quantitatively to afford **5**·Cl in 12 h (Figure S6), indicating that the coordination of the bipyridine (bpy) units to Ru^{2+} in **1** substantially reduced the reactivity of its acylhydrazine subunits. Adding CB[8] to the 1:6 solution of **1** and **2** caused significant reduction of the resolution of the ^{1}H NMR spectra (Figure S1), and 1.0 equiv. of CB[8], relative to [**1**], led to the disappearance of the O=CH signal of **2**, which supported that CB[8] accelerated the formation of the hydrazone bond and consequently formed 3D supramolecular aggregates by encapsulating the 4-phenylpyridinium dimers. After the addition of 3.0 equiv. of CB[8], the α-H signal (~9.32 ppm) of the pyridinium unit of **2** also disappeared. Since the α-H signal of the pyridinium unit of **2** in its mixture with CB[8] (0.5 equiv.) appeared at the same position (Figure S7), these observation supported that, in the mixture of **1**, **2** and CB[8] (1:6:3), **3** was formed quantitatively as a result of the formation of supramolecular network **MCSOF-1** (Figure 1).

Attenuated total reflection Fourier transform infrared spectroscopy also confirmed the quantitative formation of **3** in water (Figure S8), because in the presence of CB[8], the

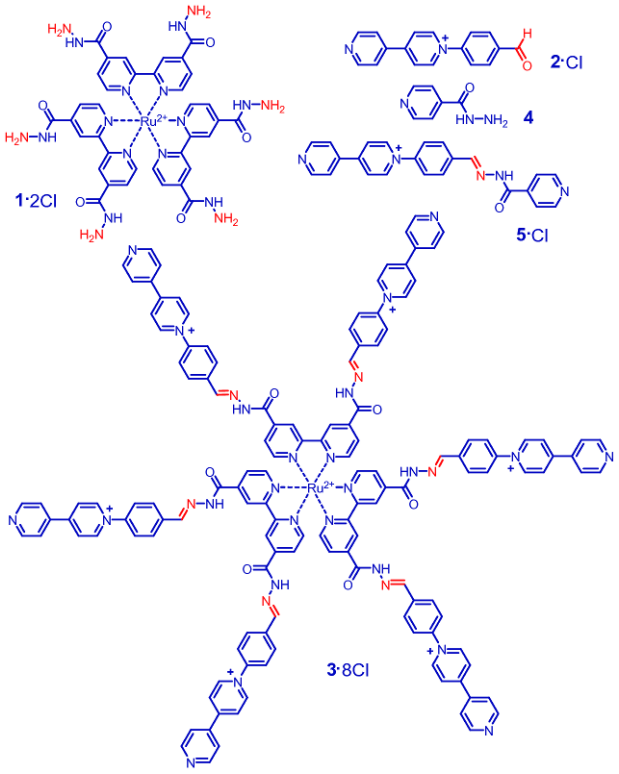

Scheme 1 The structures of compounds **1**–**5** (color online).

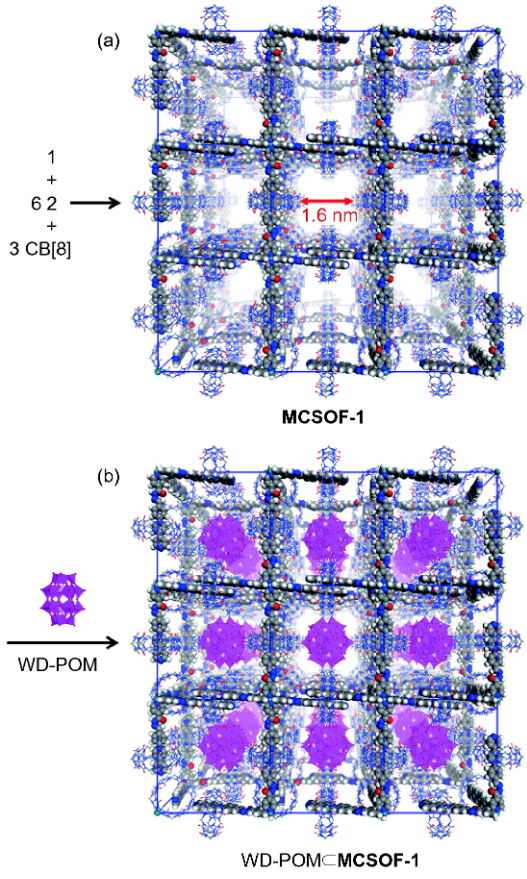

Figure 1 Formation of **MCSOF-1** (a) and WD-POM⊂**MCSOF-1** (b). The two space-filling structural models were obtained using Materials Studio 7.0. H [41] (color online).

two originally weakened diagnostic O=C−H stretching vibrations of **2** at 2852 and 2918 cm^{-1} in the solution of **1** and **2** disappeared completely. Diffusion-ordered NMR spectroscopic (DOSY) experiments for the mixture of **1**, **2** and CB[8] (1:6:3) in D_2O showed that all the signals gave rise to a similar diffusion coefficient (D, 1.2×10^{-10} m^2/s) (Figure S9), which was notably smaller than that of compound **1** (2.5×10^{-10} m^2/s) or **2** (5.0×10^{-10} m^2/s) of the identical concentration. This result supported the formation of larger supramolecular aggregates in the mixture. Dynamic light scattering (DLS) experiments revealed an average hydrodynamic diameter (D_H) of 152 nm for the supramolecular aggregates ([**1**]=0.5 mM) (Figure S10). Upon diluting the solution to [**1**]=5 μM, D_H was still as high as 121 nm (Figure S11).

Solution-phase synchrotron small-angle X-ray scattering (SAXS) experiments for the 1:6:3 solution ([**1**]=1 mM) in water revealed a broad but clear peak (Figure 2(a)), which matched with the calculated {110} spacing (2.1 nm) of the 3D cubic **MCSOF-1** (Figure 1) formed by **3** and CB[8] through the 2:1 encapsulation of the peripheral bipyridine subunits of **3** in the cavity of CB[8]. The broadness of the peak rationally reflected the dynamic nature of the new supramolecular framework in solution as well as possible defects in the framework. This dynamic nature might include the relative extension or slipping of the two aromatic units entrapped in CB[8] and/or the rotation of the 2:1 encapsulation complex unit around the two connected ruthenium complexes, both of which could lead to broadening of the scattering peak. The diffraction peak was persistent at lower concentrations ([**1**]=0.5 and 0.1 mM (Figure S12), again supporting the high stability of the new framework.

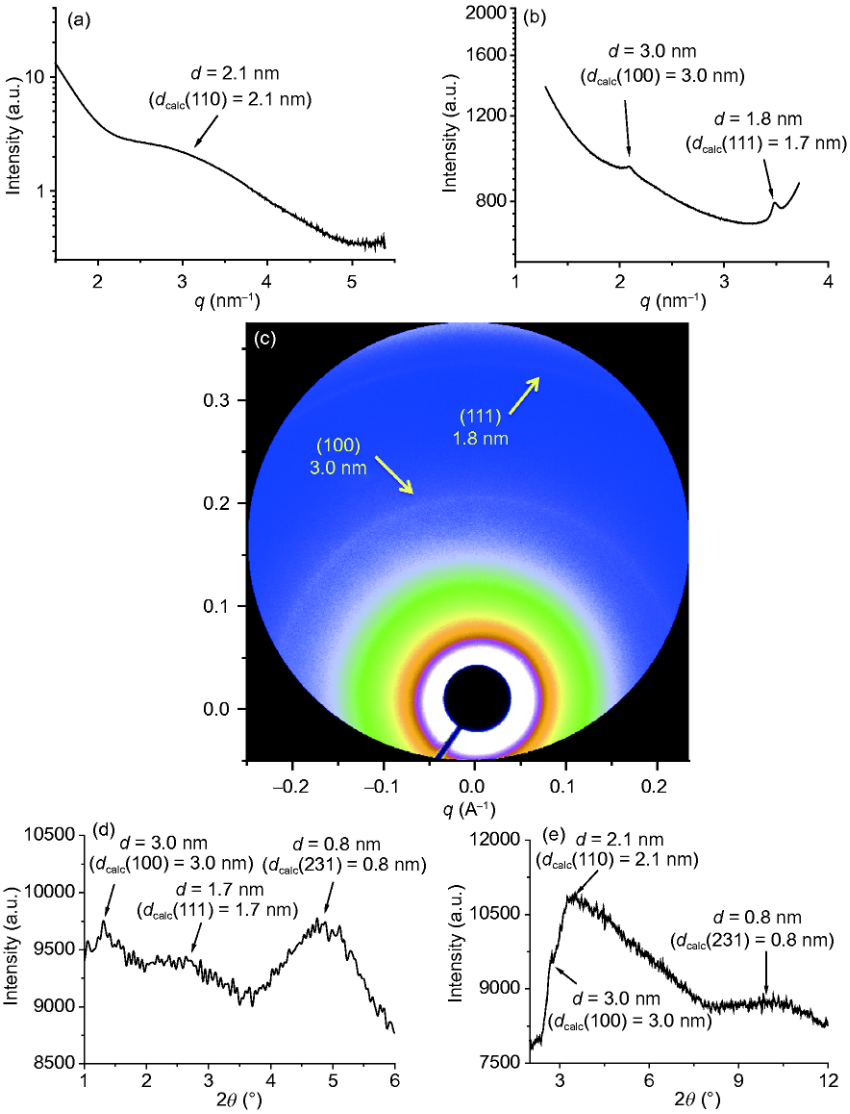

Figure 2 (a) Solution-phase synchrotron small-angle X-ray scattering profile of **MCSOF-1** ([**1**]=1 mM) in water. (b) Solid-phase synchrotron X-ray scattering profile of **MCSOF-1**. (c) 2D solid-phase synchrotron X-ray scattering profile of **MCSOF-1**. (d) Solid-phase X-ray diffraction of **MCSOF-1**. (e) Solid-phase X-ray diffraction of WD-POM⊂**MCSOF-1** [42,43] (color online).

Slow evaporation of the solution of **MCSOF-1** in water led to the formation of microcrystals (Figure S13). The synchrotron SAXS profile of the microcrystals displayed two sharp peaks centered at 3.0 and 1.8 nm (Figure 2(b)), respectively, which were also reflected on the 2D synchrotron scattering profile (Figure 2(c)). The two peaks matched with the calculated spacings of the {100} (3.0 nm) and {111} (1.7 nm) facings of the modelled framework. The X-ray diffraction (XRD) profile of the microcrystals exhibited three broad, but distinguishable peaks around 3.0, 1.7 and 0.8 nm (Figure 2(d)), respectively, corresponding to the {100}, {111} and {231} spacings of the modelled framework. Both experiments provided consistent evidences for the periodicity of **MCSOF-1** in the solid state. Elemental energy dispersive X-ray spectroscopic (EDX) mapping analysis further confirmed the compositions of the C, N, O, Ru and Cl elements of the microcrystals (Figure S14). Thermo-gravimetric analysis (TGA) showed that **MCSOF-1** has a good thermostability up to 300 °C (Figure S15).

Modelled **MCSOF-1**, including the anions, possessed about 82% of void volume. The pore aperture of the square defined by four adjacent CB[8] molecules was about 1.6 nm (Figure 1). Since complex **3** bears eight positive charges, we further studied its adsorption for redox-active Wells-Dawson polyoxometalate (WD-POM) $K_6[P_2W_{18}O_{62}]$, which has a width of 1.1 nm, in water using fluorescence spectroscopy. Adding WD-POM, which is nonfluorescent, to the solution of **MCSOF-1** ([**1**]=20 μM) led to the quenching of the fluorescence of the $Ru(bpy)_3^{2+}$ units and 1 equiv. of WD-POM could realize maximum quenching (Figure 3(a)),

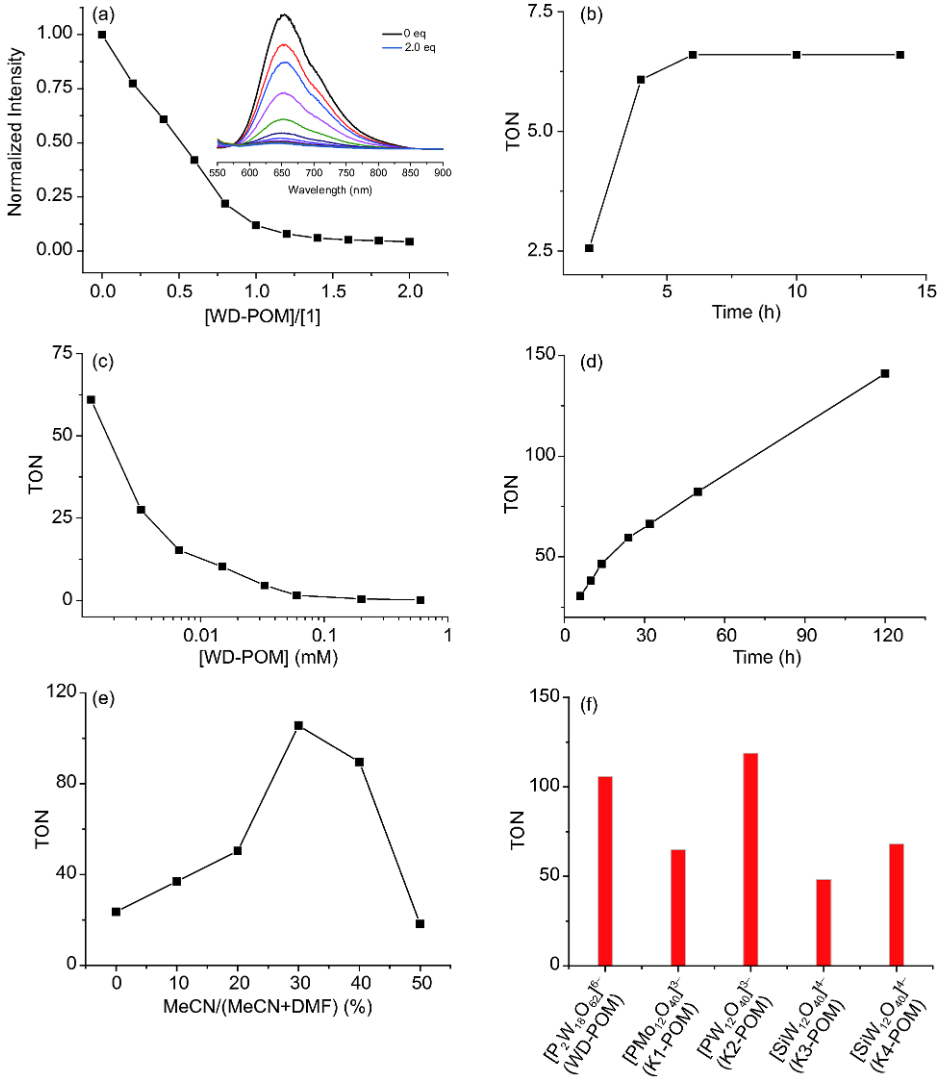

Figure 3 (a) Fluorescence quenching (λ_{max}=650 nm, λ_{ex}=500 nm) of **MCSOF-1** ([**1**]=0.02 mM) by WD-POM ([WD-POM]/[**1**]=0–2.0) in water. (b) Time-dependent TON of WD-POM@**MCSOF-1** in water ([**1**]/[WD-POM]=15, [**1**]=0.2 mM, pH 1.8) with methanol as the sacrificial electron donor. (c) TON versus [WD-POM] for heterogeneous catalysis ([**1**]/[WD-POM]=15 in solution, irradiation time=6 h). (d) Time-dependent TON of solid WD-POM@**MCSOF-1** in DMF and AcOH (0.1 M) with NEt_3 as sacrificial electron donor ([**1**]/[WD-POM]=15. (e) TON versus MeCN% in binary DMF and MeCN containing AcOH (0.1 M) with NEt_3 as sacrificial electron donor ([**3**]/[WD-POM]=15, irradiation time=10 h). (f) TON of different POMs in binary DMF and MeCN (7:3, *v*/*v*) containing AcOH (0.1 M) with NEt_3 (1 M) as sacrificial electron donor ([**3**]/[POM]=15, irradiation time=10 h) (color online).

which indicated that the adsorption of WD-POM by **MCSOF-1** occurred in a manner such that one cubic cage of **MCSOF-1** encapsulated one WD-POM anion. This one-cage-one-guest adsorption mode was further confirmed by the inductively coupled plasma-atomic emission spectrometry (ICP-AES) analysis, which revealed a Ru/W atomic ratio of 0.056 that was equal to the calculated value for WD-POM⊂**MCSOF-1**. After 3 d of dialysis ([**1**]=0.5 mM) using a membrane filter with a molecular weight cutoff of 1.0 kD, which allowed for the diffusion of both free WD-POM and **2**, ICP-AES analysis showed that the Ru/W atomic ratio was unchanged. Dialysis experiments also revealed that only ca. 1% of **2** diffused into the outside water. Both results supported that WD-POM was tightly held by the framework even at very low concentration. DLS revealed that the adsorption of WD-POM caused D_H of **MCSOF-1** to increase from 156 to 1420 nm (Figure S10). This remarkable size increase might be rationalized by considering that the adsorbed POMs further stabilized the framework through electrostatic interaction or acted as linkers to induce further aggregation of the frameworks. The XRD profile of the solid sample of WD-POM⊂**MCSOF-1** exhibited three peaks at 3.0, 2.1, and 0.8 nm (Figure 2(e)), which respectively corresponded to the {100}, {110} and {231} spacings of modeled **MCSOF-1**. The SAXS profile of the solid sample of WD-POM⊂**MCSOF-1** also gave rise to two weak but discernible peaks at 1.7 and 1.5 nm (Figure S16), which could be assigned to the {111} and {200} spacings of the modeled framework. Both results supported that, after adsorption of WD-POM, **MCSOF-1** maintained its periodicity.

Excited $[Ru(bpy)_3]^{2+}$ has been revealed to undergo multiple electron injection to WD-POM to initiate the catalysis of WD-POM for the reduction of proton into H_2 [14,44]. The highest occupied molecular orbital energy of **MCSOF-1** and the lowest unoccupied molecular orbital energy of WD-POM were determined to be −5.84 and −4.78 eV, respectively (Figure S17 and Table S1, Supporting Information online). The maximum absorption of **MCSOF-1** in the visible range appeared around 476 nm (Figure S18). We thus selected the visible light (500 nm) as excitation to study the efficiency of WD-POM@**MCSOF-1** for the photocatalytic reduction of proton to produce H_2. The reactions were performed in an acidic aqueous solution (pH 1.8), using methanol as the sacrificial electron donor. For the first series of experiments, the concentration of **MCSOF-1** was kept at [**1**]=0.3 mM and the irradiation time was kept for 6 h. The efficiency of H_2 production was investigated in the presence of varying amounts of WD-POM (up to 0.6 mM). It was found that at [WD-POM]=0.0013 mM ([**3**]/[WD-MOF]=15), the turnover number (TON) for H_2 production, which was defined as n(1/2H_2)/n(WD-POM), reached 61 (Figure S19). Further decrease of the concentration of WD-POM led to the increase of TON, but the amount of H_2 produced to decrease. In the absence of CB[8], irradiating the mixture solution of **1**·2Cl, **2**·Cl (1:6) and WD-POM of different concentrations did not produce any H_2, which confirmed the necessity of the enrichment of **MCSOF-1** for WD-POM in enabling the catalysis [45]. At a constant concentration of **MCSOF-1** ([**1**]= 0.3 mM) and WD-POM (0.02 mM), TON reached maximum after irradiation for about 6 h (Figure 3(b)). By keeping [**3**]/[WD-POM]=15 and 6 h irradiation, reducing their concentration gave rise to increased TONs (Figure 3(c)), and at [WD-POM]=0.0013 mM, TON reached 61, furthering showing the remarkable capacity of **MCSOF-1** in enriching WD-POM.

Heterogeneous photocatalytic H_2 production by WD-POM⊂**MCSOF-1** was further investigated. The POM-loaded solid sample ([**1**]/[WD-POM]=15) was insoluble in DMF. Its catalytic activity was thus exploited in DMF containing 0.1 M of acetic acid, with triethylamine (1 M) as the sacrificial electron donor (Figure 3(d) and Table S2). TON reached 141 after irradiating for 120 h. As observed in solution, at the fixed amount of **MCSOF-1**, reducing the amount of WD-POM resulted in increased TON, and adding acetonitrile (up to 40 *v*%) to the solution considerably facilitated the production of H_2 (Figure 3(e) and Table S3).

Fluorescence experiments revealed that **MCSOF-1** also adsorbed Keggin-type POMs $K_3[PMo_{12}O_{40}]$ (K1-POM), $K_3[PW_{12}O_{40}]$ (K2-POM), $K_4[SiW_{12}O_{40}]$ (K3-POM), and $K_4[SiMo_{12}O_{40}]$ (K4-POM) (Figure S20). Evaporation of their homogeneous solutions ([**3**]/[POM]=15) afforded four solid catalysts. In the DMF/acetonitrile mixture (3:7, *v*/*v*), all the four samples could catalyze visible light-induced reduction of proton to afford H_2 (Figure 3(f) and Table S4), with $[PW_{12}O_{40}]^{3-}$ displaying the highest activity that surpasses that of WD-POM.

3 Conclusions

In summary, we have demonstrated that three molecular components can react and self-assemble to generate hybridized periodic framework, which features porous metal, covalent and supramolecular organic frameworks. This self-assembled framework hybrid maintains periodicity in both solution and the solid state and is highly stable in water. The fact that discrete polyoxametallates can be adsorbed by the framework at very low concentrations to realize efficient visible light-induced reduction of proton to generate hydrogen illustrates that the guests are orientated in an identical ordered pattern in the 3D space, which, to some extent, mimics the structural feature of photosynthetic systems. This self-assembly strategy offers new possibility for constructing integrated hybrid materials by replacing the $[Ru(bpy)_3]^{2+}$ with non-noble metal complexes or using other photo-active guest catalysts.

Acknowledgements This work was supported by the National Natural Science Foundation of China (21529201, 21432004, 91527301), the Molecular Foundry, Lawrence Berkeley National Laboratory, and the Office of Science, Office of Basic Energy Sciences, Scientific User Facilities Division, of the U.S. Department of Energy (DE-AC02- 05CH11231). We thank the Shanghai Synchrotron Radiation Facility for providing BL16B1 and BL14B1 beamlines for collecting the synchrotron X-ray scattering and diffraction data, and the SIBYLS Beamline 12.3.1 of the Advanced Light Source, Lawrence Berkeley National Laboratory, for collecting solution-phase synchrotron small-angle X-ray scattering data.

Conflict of interest The authors declare that they have no conflict of interest.

Supporting information The supporting information is available online at http://chem.scichina.com and http://link.springer.com/journal/11426. The supporting materials are published as submitted, without typesetting or editing. The responsibility for scientific accuracy and content remains entirely with the authors.

1 MacGillivray LR, Lukehart CM, ed. *Metal-Organic Framework Materials*. Singapore: Pan Stanford Publishing Ltd., 2015. 563
2 Feng X, Ding X, Jiang D. *Chem Soc Rev*, 2012, 41: 6010–6022
3 Ding SY, Wang W. *Chem Soc Rev*, 2013, 42: 548–568
4 Yuan F, Tan J, Guo J. *Sci China Chem*, 2018, 61: 143–152
5 Yang T, Cui Y, Chen H, Li W. *Acta Chim Sin*, 2017, 75: 339–350
6 Wu MX, Yang YW. *Chin Chem Lett*, 2017, 28: 1135–1143
7 Wang H, Zhang DW, Li ZT. *Acta Polym Sin*, 2017, 1: 19–26
8 Liu G, Sheng J, Zhao Y. *Sci China Chem*, 2017, 60: 1015–1022
9 Ma L, Wang S, Feng X, Wang B. *Chin Chem Lett*, 2016, 27: 1383–1394
10 Liu XH, Guan CZ, Wang D, Wan LJ. *Adv Mater*, 2014, 26: 6912–6920
11 Wang H, Ding H, Meng X, Wang C. *Chin Chem Lett*, 2016, 27: 1376–1382
12 Wang Q, Xiong S, Xiang Z, Peng S, Wang X, Cao D. *Sci China Chem*, 2016, 59: 643–650
13 Zhang KD, Tian J, Hanifi D, Zhang Y, Sue ACH, Zhou TY, Zhang L, Zhao X, Liu Y, Li ZT. *J Am Chem Soc*, 2013, 135: 17913–17918
14 Tian J, Zhou TY, Zhang SC, Aloni S, Altoe MV, Xie SH, Wang H, Zhang DW, Zhao X, Liu Y, Li ZT. *Nat Commun*, 2014, 5: 5574
15 Tian J, Xu ZY, Zhang DW, Wang H, Xie SH, Xu DW, Ren YH, Wang H, Liu Y, Li ZT. *Nat Commun*, 2016, 7: 11580
16 Wu YP, Yang B, Tian J, Yu SB, Wang H, Zhang DW, Liu Y, Li ZT. *Chem Commun*, 2017, 53: 13367–13370
17 Pfeffermann M, Dong R, Graf R, Zajaczkowski W, Gorelik T, Pisula W, Narita A, Müllen K, Feng X. *J Am Chem Soc*, 2015, 137: 14525–14532
18 Zhang Y, Zhan TG, Zhou TY, Qi QY, Xu XN, Zhao X. *Chem Commun*, 2016, 52: 7588–7591
19 Xu SQ, Zhang X, Nie CB, Pang ZF, Xu XN, Zhao X. *Chem Commun*, 2015, 51: 16417–16420
20 Li Y, Dong Y, Miao X, Ren Y, Zhang B, Wang P, Yu Y, Li B, Isaacs L, Cao L. *Angew Chem Int Ed*, 2018, 57: 729–733
21 Ko YH, Kim E, Hwang I, Kim K. *Chem Commun*, 2007, 35: 1305–1315
22 Liu Y, Yang H, Wang Z, Zhang X. *Chem Asian J*, 2013, 8: 1626–1632
23 Isaacs L. *Acc Chem Res*, 2014, 47: 2052–2062
24 Das D, Scherman OA. *Isr J Chem*, 2011, 51: 537–550
25 Biedermann F, Nau WM, Schneider HJ. *Angew Chem Int Ed*, 2014, 53: 11158–11171
26 Tian J, Chen L, Zhang DW, Liu Y, Li ZT. *Chem Commun*, 2016, 52: 6351–6362
27 Tian J, Zhang L, Wang H, Zhang DW, Li ZT. *Supramol Chem*, 2016, 28: 769–783
28 Wang R, Qiao S, Zhao L, Hou C, Li X, Liu Y, Luo Q, Xu J, Li H, Liu J. *Chem Commun*, 2017, 53: 10532–10535
29 De Greef TFA, Smulders MMJ, Wolffs M, Schenning APHJ, Sijbesma RP, Meijer EW. *Chem Rev*, 2009, 109: 5687–5754
30 Guo DS, Liu Y. *Chem Soc Rev*, 2012, 41: 5907
31 Yan X, Wang F, Zheng B, Huang F. *Chem Soc Rev*, 2012, 41: 6042
32 Barrow SJ, Kasera S, Rowland MJ, del Barrio J, Scherman OA. *Chem Rev*, 2015, 115: 12320–12406
33 Wang Q, Cheng M, Cao Y, Jiang J, Wang L. *Acta Chim Sin*, 2016, 74: 9–16
34 Xiong C, Sun R. *Chin J Chem*, 2017, 35: 1669–1672
35 Yin ZJ, Wu ZQ, Lin F, Qi QY, Xu XN, Zhao X. *Chin Chem Lett*, 2017, 28: 1167–1171
36 Wang Q, Cheng M, Jiang JL, Wang LY. *Chin Chem Lett*, 2017, 28: 793–797
37 Li H, Wang J, Ni Y, Zhou Y, Yan D. *Acta Chim Sin*, 2016, 74: 415–421
38 Yang L, Tan X, Wang Z, Zhang X. *Chem Rev*, 2015, 115: 7196–7239
39 Tian J, Yao C, Yang WL, Zhang L, Zhang DW, Wang H, Zhang F, Liu Y, Li ZT. *Chin Chem Lett*, 2017, 28: 798–806
40 Yao C, Tian J, Wang H, Zhang DW, Liu Y, Zhang F, Li ZT. *Chin Chem Lett*, 2017, 28: 893–899
41 Materials Studio 7.0, Accelrys Software Inc., San Diego, USA
42 Yang TY, Wen W, Yin GZ, Li XL, Gao M, Gu YL, Li L, Liu Y, Lin H, Zhang XM, Zhao B, Liu TK, Yang YG, Li Z, Zhou XT, Gao XY, *Nucl Sci Tech*, 2015, 26: 020101
43 Zeng J, Bian F, Wang J, Li X, Wang Y, Tian F, Zhou P. *J Synchrotron Rad*, 2017, 24: 509–520
44 Zhang ZM, Zhang T, Wang C, Lin Z, Long LS, Lin W. *J Am Chem Soc*, 2015, 137: 3197–3200
45 Wang F, Liang WJ, Jian JX, Li CB, Chen B, Tung CH, Wu LZ. *Angew Chem Int Ed*, 2013, 52: 8134–8138